ELSEVIER

Thermochimica Acta 304/305 (1997) 99–110

thermochimica acta

Heat capacity spectroscopy at the glass transition in polymers

J. Korus*, M. Beiner, K. Busse, S. Kahle, R. Unger, E. Donth

Universität Halle, Fachbereich Physik, D-06099 Halle/Saale, Germany

Received 2 August 1996; accepted 12 December 1996

Abstract

A heat capacity spectroscopy HCS setup (3ω method) adapted to measure glass transitions in polymers is described. Sample contacting and signal sensitivity are improved so that the relevant complex heat capacity in a (0.2–2000) Hz frequency region can be recorded down to relative heat capacity steps $\Delta c_p/c_p$ of a few percent. Linearity and Kramers–Kronig consistency tests are described. The influence of heater width and sample thickness is discussed. The possibilities of the instrument are demonstrated for the glass transition in natural rubber, polystyrene, and a random copolymer of *n*-butyl methacrylate and styrene. © 1997 Elsevier Science B.V.

Keywords: Heat capacity spectroscopy; Natural rubber; Poly(*n*-butyl methacrylate-*stat*-styrene) copolymers ; Polystyrene

1. Introduction

Heat capacity spectroscopy HCS [1] is a useful tool for the investigation of dynamic glass transition. The aim is to determine dynamic or complex heat capacity $c_p^* = c_p' - ic_p''$ [2] as a function of frequency and temperature above the glass temperature T_g in thermal equilibrium. In contrast to the temperature-modulated DSC (TMDSC) in the ramp regime [3,4], HCS is not affected by structural relaxation, i.e. by an interference of equilibrium and non-equilibrium aspects of the glass transition. Direct comparison of HCS data with those from other relaxation spectroscopy methods such as dielectric or shear measurements is possible [5–8]. Nevertheless, up to now only a very small number of glass formers have been investigated by this method. The reasons are specific experimental problems of the HCS method. Three main problems of the so-called 3ω technique [1,9–11] are: (i) it is difficult to extract the very small electric signals (two lock-in amplifiers for $U(\omega)$ and $U(3\omega)$ signals, linearity of the frequency tripler over a wide frequency range); (ii) the high $\rho\kappa c_p$ value (ρ – material density, κ – thermal conductivity) of the window-glass substrate can dominate over the $\rho\kappa c_p$ value of the sample to be measured; and (iii) realization of a good heater–sample contact during density changes. In order to enlarge the number of substances investigable by HCS, it is necessary to make progress with the experimental problems; especially, to optimize the signal-to-noise ratio and to compensate the internal stress of the samples.

The aim of this paper is to describe several modifications of our experimental HCS setup as compared to the devices used by other authors [9,10]. The influence of finite size effects on c_p^* data is also discussed. The progress made in experimental sensi-

*Corresponding author.

PII S0040-6031(97)00028-2

tivity and stability is demonstrated for three polymeric glasses: natural rubber (NR), polystyrene (PS), and a statistical copolymer, where the signal at the dynamic glass transition is smaller than those of the previously measured glass formers like glycerol [1], propylene glycol [11] or *ortho*-terphenyl [12].

2. Experimental setup and data evaluation method

The basic equation for HCS is the one-dimensional heat diffusion equation in the frequency domain,

$$\kappa \frac{\partial^2 T(x,\omega)}{\partial x^2} = -i\omega\rho c_p T(x,\omega) \tag{1}$$

where ρ is the mass density, κ the thermal conductivity of the medium surrounding the heater, and x and ω the position and frequency variables, respectively. Generally, both heat capacity, c_p^* [2], and thermal conductivity, κ^*, should be considered to be complex. At the dynamic glass transition, c_p^* depends on both the frequency of the temperature perturbation and the underlying stationary temperature.

In order to produce a periodic temperature perturbation of frequency ω, the following technique is used: An alternating current of frequency $\omega/2$ is applied to a thin heater. The thermal properties of the surroundings modulate the alternating current; Subsequently, a third harmonic will be generated [13] (3ω method). This third harmonic can be detected by a frequency selective setup.

Assuming a plane heater with infinitesimal thickness but large in size, surrounded by the sample on one side and a substrate on the other side, the solution of the heat diffusion equation (Eq. (1)) is [9,10,7]

$$\Delta T^*(\omega, x=0) = \frac{P_0}{A(\kappa k^* + \kappa_S k_S^*)} \tag{2}$$

where ΔT^* is the complex temperature oscillation at the heater surface ($x = 0$), A the heater area, and P_0 the heating power. The $k^* = \sqrt{-i\omega c_p^* \rho/\kappa}$ and k_S^* values are the complex thermal wave vectors for the sample and the substrate (index S), respectively.

If we use a substrate without any relaxation in the temperature range of interest (i.e. c_{pS} and κ_S are assumed to be real) the third harmonic component of the voltage across the heater is given by

$$U_{3\omega} e^{i\varphi} = \frac{R_2}{R_2 + R_0} \cdot \frac{\alpha I_0^3 R_0^2}{2A\sqrt{\omega}} e^{i\frac{\pi}{4}} \times \left(\sqrt{\rho_S \kappa_S c_{pS}} + \sqrt{\rho |(\kappa c_p)^*|} e^{i\delta/2} \right)^{-1} \tag{3}$$

where $U_{3\omega}$ and φ are the amplitude and phase shift of the third harmonic, I_0, R_0, and α, respectively, the amplitude of the input current, the resistance of the heater at a given temperature, and the temperature coefficient of resistivity, $|(\kappa c_p)^*|$ and δ the amplitude and phase of the complex product $(\kappa c_p)^*$ for the sample.

If the $\rho_S \kappa_S c_{pS}$ product for the substrate is not too large as compared to $\rho\kappa c_P$ for the sample, then it follows from Eq. (3) that the $U_{3\omega}^*$ signal for a given sample mainly depends on its own $\rho\kappa c_P^*$ behavior (i.e. on its mean absolute $(\overline{\rho\kappa c_p})'$ value at the dynamic glass temperature, the relative glass-transition step height $\Delta(\rho\kappa c_p)'/(\overline{\rho\kappa c_p})'$, and the $\tan\delta = (\kappa c_p)''/(\kappa c_p)'$ value at the dynamic glass transition). On the other hand, the choice of a suitable substrate is important for the efficiency of a HCS device.

In order to enlarge the sensitivity and stability of HCS experiments we used a modified setup operating in the (0.2–2) kHz frequency range (Fig. 1). Details and the cryogenics will be described in Ref. [14]. The main differences are:

1. We used a polymer substrate instead of window glass. Polymers such as epoxy resins or polyetheretherketone (PEEK) have $\rho\kappa c_p$ values which are very small compared with those of window glass ($\rho\kappa c_p$(PEEK) $\approx 4.5 \times 10^{-3}$ J^2/(cm^4 K^2 s), $\rho\kappa c_p$(glass)$\approx 50 \times 10^{-3}$ J^2/(cm^4 K^2 s)). This decreases the substrate term in Eq. (3) with the result that the total signal becomes more sensitive to the properties of the sample.
2. The lock-in amplifiers and the frequency tripler [9] are substituted by a digital scope and a selective Fourier transformation. The time-dependent voltage data were accumulated by the oscilloscope, transferred to a computer and fitted to a superposition of first and third harmonic components according to the theoretical prediction for the equilibrated bridge. This technique significantly increases the precision of the phase shift determi-

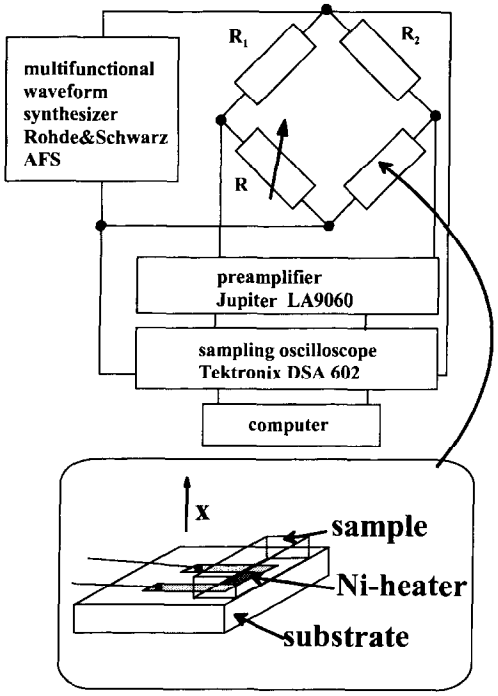

Fig. 1. Schematic diagram of the experimental setup. The inset shows the geometry of substrate, heater and sample.

nation. We have reached a phase angle sensitivity of 0.02° ... 0.04°.

Some additional effort was necessary to balance the Wheatstone bridge automatically and to realize a continuous contact between polymeric sample and heater. The bridge balance was realized by an on-line Fourier technique. The $U_\omega/U_{3\omega}$ peak-height ratio at 1 kHz was minimized using a fast Fourier transformation (FFT) of the signal. The polymeric samples were prepared as follows: A thin (≈1.5 mm) sheet of the sample was placed on the heater and, subsequently, heated into the molten state. Then the sample was slowly cooled and held under slight pressure during the isothermal frequency sweeps. The measurement was started at the highest temperature. In this way, the probability that the sample separates from the heater near T_g is relatively small (ca. 50%).

An additional increase of the signal amplitude was reached by using relatively small heater areas of about $A \approx 1 \times 4\,\mathrm{mm}^2$. This increases the temperature amplitude ΔT and, therefore, the voltage $U_{3\omega}$ for a given sample (Eq. (3) and Eq. (4)). Typical values for $\nu \equiv \omega/2\pi = 20$ Hz are $\Delta T = 0.75$ K and $U_{3\omega} = 0.6$ mV. The heater resistance was always $R \approx 30\,\Omega$ at room temperature. The use of small heaters and relatively thin samples has, however, the disadvantage of finite size effects at low frequencies, where the thermal wave length $\lambda = |k^*|^{-1} = \sqrt{\kappa/(\omega\rho c_p)}$ becomes comparable with the heater and sample dimensions. The effects of both finite heater width and finite sample thickness on the temperature wave propagation in the sample will be discussed in Section 3 of this paper.

Fig. 2 shows a typical set of raw data from our device: the output voltage in the time and frequency domain. The theoretical ratio (1 : 1) between U_ω and

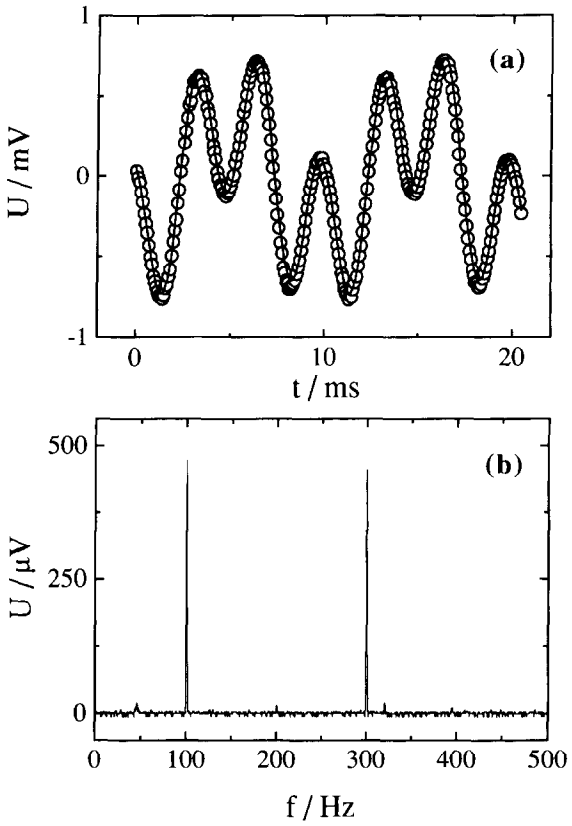

Fig. 2. Raw voltage data from the equilibrated Wheatstone bridge in the (a) – time and (b) – frequency domain. The solid line in (a) is a fit to the data with $U(t) = U_\omega \cos(\omega t/2) + U_{3\omega}\cos(3\omega t/2 + \varphi)$. The signal in (b) was taken from a fast Fourier transform of 200 cycles of the time signal in (a). The data are for polyvinylacetate at 90°C.

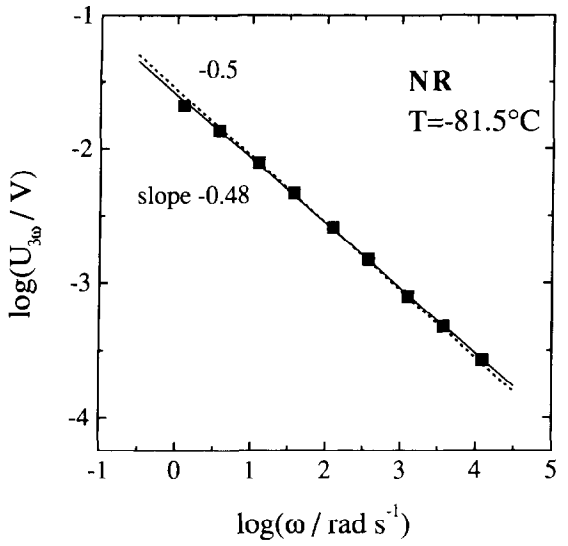

Fig. 3. Logarithm of signal voltage $\log U_{3\omega}$ vs. logarithm frequency $\log\omega$ for natural rubber at $T = -81.5°C$ (outside the dynamic glass transition). The solid line is a log–log linear fit of the data. The dotted line gives the theoretical value of −0.5 from Eq. (3).

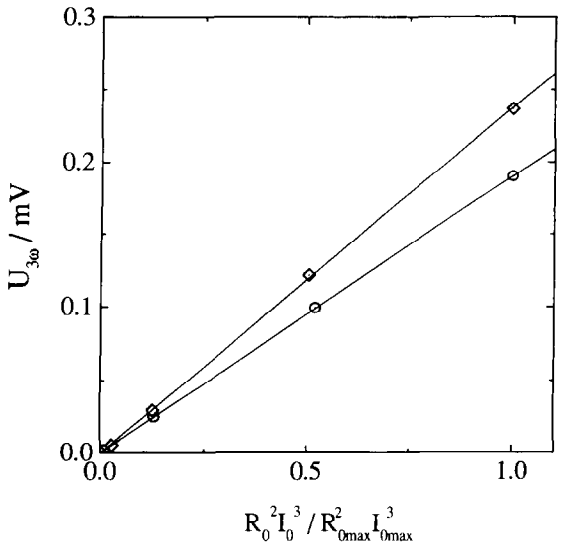

Fig. 4. The signal voltage $U_{3\omega}$ *vs* normalized power-related constant $R_0^2 I_0^3 / R_{0max}^2 I_{0max}^3$ of Eq. (3) for (○) – polystyrene and (◇) – poly(*n*-octyl methacrylate) outside the dynamic glass transition. The given data were obtained at a frequency of 2 kHz and demonstrate the linearity of response.

$U_{3\omega}$ amplitudes was obtained for the equilibrated bridge. The $U(t)$ data in Fig. 2(a) can be fitted by a superposition of two sinusoidal components according to the modification (ii) described here.

Our experimental setup was also checked with respect to the $1/\sqrt{\omega}$ dependence of Eq. (3) and to the linear response behavior [7]. The frequency dependence of the third harmonic signal $U_{3\omega} \sim \omega^{-1/2}$ is verified in Fig. 3, and the invariance of the $U_{3\omega}^* \sim ((\rho\kappa c_p)^*)^{-1/2}$ results against a moderate variation of the power amplitude (presented here as the $R_0^2 I_0^3 / (R_{0max}^2 I_{0max}^3)$ ratio, in accordance with Eq. (3)) in Fig. 4.

In general, no large deviations from the expected behavior are observed. The reason for slight differences between the theoretical and experimental frequency exponent m ($\omega^{-0.48}$ instead of $1/\sqrt{\omega} = \omega^{-0.5}$) remains an open question. The exponent m seems to be dependent on the heater preparation and was always greater than −0.5, usually in the −0.43...−0.48 range. Deviations of the φ base line from the theoretical $\pi/4$ value (Eq. (4)), and a displacement of the φ base line in the dynamic glass-transition region, especially at frequencies below 20 Hz, are probably a consequence of the finite heater width. These effects will be discussed in some detail in Section 3. A quantitative compensation according to the equations of Section 3 is not easy to assess, and will be the scope of a future work. An experimental way out seems to be the use of a cascade of heaters, each optimized for a special frequency range (large heaters for low frequencies and small heaters for high frequencies). But this method would be very time-consuming, and the calibration requirements be very high.

The $(\rho\kappa c_p)^*$ data were calculated from the raw $U_{3\omega}$ and φ data in a way that also differs in detail from Eq. (3):

(a) The $|(\rho\kappa c_p)^*|$ amplitude was calculated from $U_{3\omega}(\omega)$ by using the actual exponent m (−0.43...−0.48), evaluated from the frequency dependence outside the dynamic glass-transition region and not from the theoretical proportionality $U_{3\omega} \sim \omega^{-1/2}$. This was simply realized in a first-order approximation by fixing all isochrones to the 20 Hz curve at a high temperature equilibrium point outside the dynamic glass transition (vertical shift). This leads to a divergence of the low-temperature $(\rho\kappa c_p)'$ values.

(b) The imaginary part $(\rho\kappa c_p)''$ was obtained from the experimental φ values by substraction of the φ base line outside the dynamic glass transition. The

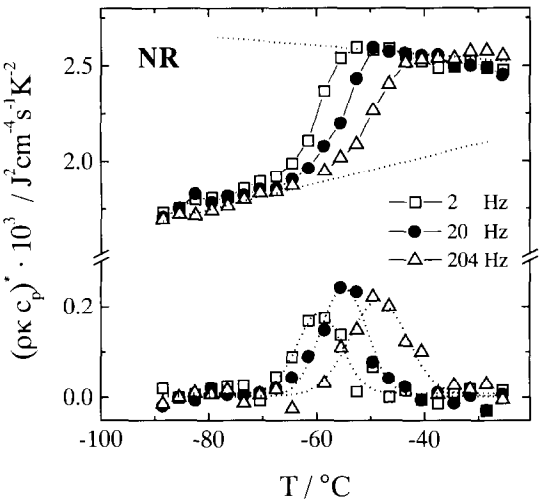

Fig. 5. The real (upper) and imaginary (lower) parts of the complex isochronal HCS output $(\rho\kappa c_p)^*$ for natural rubber (NR) as a function of temperature. The dotted lines in the lower part are fits to the $(\rho\kappa c_p)''$ data with a Gaussian function. The solid lines in the upper part are only guides for the eye.

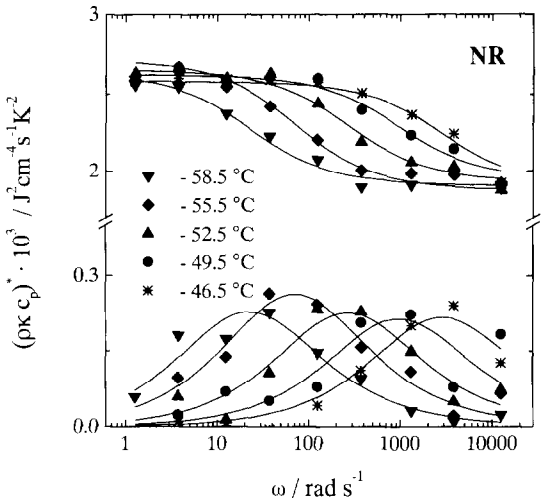

Fig. 6. The real (upper) and imaginary (lower) parts of $(\rho\kappa c_p)^*$ isotherms in natural rubber as a function of frequency. The lines in the lower part are fits of $(\rho\kappa c_p)''$ data with a Havriliak–Negami function. The lines in the upper part were calculated using the same HN parameter set and an additive constant $\rho\kappa c_{p\infty}$. The small deviations in the upper part demonstrate the consistence of a Kramers–Kronig consistency test.

typical $\varphi(\omega)$ values at high frequencies are very close to the theoretical value of $\pi/4$. At low frequencies (< 20 Hz), the deviations are much larger (up to 15° at 0.2 Hz, see, e.g. Fig. 7, below). Simultaneously the low- and high-temperature plateau values outside the dynamic glass transition became different. This behavior limits the available $(\rho\kappa c_p)''$ frequency range of our experimental setup to $\nu = \omega/2\pi \geq 0.1$ Hz.

The $(c_p\rho\kappa)''$ Gaussian-fit maximum temperature (glass temperature at a given frequency) is named here T_ν.

Representative plots of $(\rho\kappa c_p)^*$ isochrones as function of temperature for a natural rubber sample (NR, Continental AG, $T_g = -68$°C) are shown in Fig. 5. The curves show the typical behavior of a compliance at the dynamic glass transition, i.e. a steplike transformation from lower $(\rho\kappa c_p)'$ values at temperatures below the dynamic glass-transition temperature T_ν to higher values above, a corresponding peak in the imaginary part $(\rho\kappa c_p)''$, and a frequency-dependent shift of $T_\nu(\omega)$ according to the Williams–Landel–Ferry (WLF) [29] equation.

The isotherms for the natural rubber (NR) sample are presented in Fig. 6. The validity of the Kramers–Kronig relation between real and imaginary parts of $(\rho\kappa c_p)^*$ was verified in the following way. The $(\rho\kappa c_p)''$ data were fitted to the imaginary part of a complex Havriliak–Negami (HN) [30] function, $c_p^* - c_{p\infty} = \Delta c_p(1 + (i\omega/\omega_{HN})^\beta)^{-\gamma}$. β and $-\beta\gamma$ are the low- and high-frequency flank slopes of the $\log(\rho\kappa c_p)''$ vs. $\log\omega$ diagram far away from the $(\rho\kappa c_p)''$ maximum. Using the parameters obtained and an additive constant, $(\rho\kappa c_p)_\infty$, we calculated the real part of the HN function. The calculated curves and the experimental $(\rho\kappa c_p)'$ data are in good agreement as shown in Fig. 6 for NR and Fig. 11 for PS, below. The confirmation of the Kramers–Kronig relation is a strong support for the preposition that our HCS regime corresponds to linear response. Inversely, starting from the Kramers–Kronig relation, this agreement can serve as an experimental consistency test of the independently measured real and imaginary parts. Further details to this point see below, at Fig. 11.

A central problem of the 3ω method is the decoupling of $\rho\kappa$ and c_p^* [12]. The property of interest is usually $c_p^*(\omega, T)$. In the scheme of linear response, the frequency-dependent heat capacity corresponds to an entropy compliance which is, via the fluctuation dissipation theorem (FDT), directly connected with the

natural entropy (not enthalpy) fluctuations in the sample (see for example [15]). As a first approximation, we might assume that $\rho\kappa(\omega, T)$ is real and constant, because the relative changes of the thermal conductivity $\kappa(T,\omega)/\bar{\kappa}$ across the dynamic glass transition for *o*-terphenyl [12] and glycerol [11] are small compared to the $\Delta c_p/\bar{c}_p$ change. Another argument is that usually a good agreement between the HCS $\Delta(\rho\kappa c_p)'/(\overline{\rho\kappa c_p})'$ ratio and the DSC $\Delta c_p/\bar{c}_p$ ratio is observed. For natural rubber the difference between $\Delta(\rho\kappa c_p)'/(\overline{\rho\kappa c_p})'$ and $\Delta c_p/\bar{c}$ is smaller than 5%.

Nevertheless, the best way would be an experimental decoupling of ρc_p^* and κ. For this purpose Nagel et al. [12] used HCS experiments with thin plane heaters of different widths and analyzed deviations from the asymptotic behavior. Birge [11] reports on combined HCS measurements with a plane heater and a thin wire. Both methods detect signals which depend in a different way on κ and c_p^*. A comparison of both experiments, in principle, allows the decoupling of heat capacity and thermal conductivity. An alternative way is indicated by the interpretation of finite sample-thickness effects.

3. Influence of layer width and sample thickness

Originally the HCS theory was proposed for two simple cases: an infinite planar heater with zero thickness and a wire with infinite length and zero diameter. In both cases, the surroundings are assumed to be totally filled with the sample (the substrate). This means that both heater width and sample (or substrate) thickness should be very large as compared to the thermal wave length $\lambda \sim \sqrt{\kappa/\omega\rho c_p}$. In particular, at very low frequencies this assumption may be invalid, because heater and sample have finite dimensions for practical reasons.

A theoretical approach to the plane heater problem with finite heater width was described by Bae et al. in Ref. [16]. The result for the temperature amplitude is

$$\Delta T = \frac{P_0}{A\pi\kappa}\int_0^\infty \frac{\sin(ab)}{(ab)^2\sqrt{a^2+k^2}}\,\mathrm{d}a \qquad (4)$$

where A is the heater area, $2b$ the heater width and a an integration variable. The heater is here assumed to be completely surrounded by the sample. The resulting

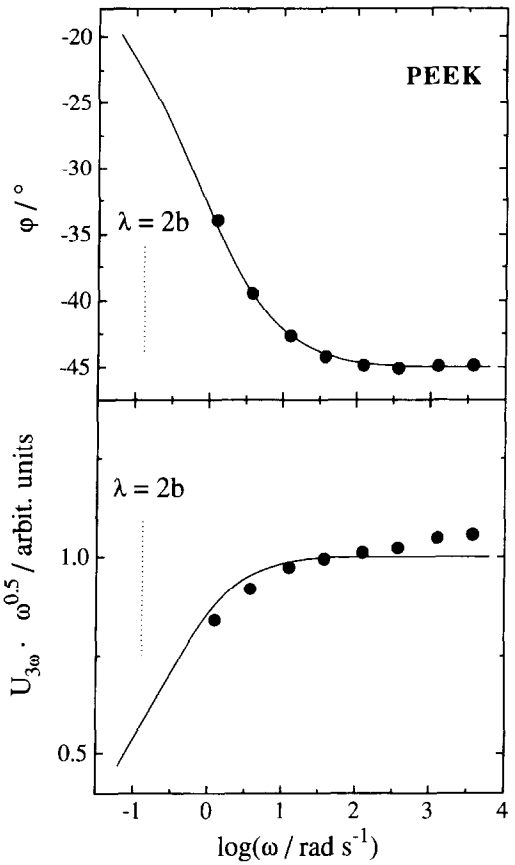

Fig. 7. The frequency dependence of the phase shift φ and the signal amplitude $U_{3\omega}$ for a Ni heater with a width of $2b = 1.2$ mm on a PEEK substrate at $T = -100$°C. The solid lines are calculated using Eq. (13) with $(\rho c_p)_S = 1.34\,\mathrm{J\,cm^{-3}\,K^{-1}}$ and $\kappa_S = 2.5\times 10^{-3}\,\mathrm{J\,cm^{-1}\,K^{-1}\,s^{-1}}$. The $\lambda = 2b$ positions are indicated by dotted lines.

third harmonic is

$$U_{3\omega}e^{i\varphi} = \frac{R_2}{R_2+R_0}\cdot\frac{\alpha I_0^3 R_0^2}{2A\pi\kappa}\int_0^\infty \frac{\sin(ab)}{(ab)^2\sqrt{a^2+k^2}}\,\mathrm{d}a \qquad (5)$$

Eq. (5) shows that both the amplitude $U_{3\omega}$ and the phase shift φ are influenced by the heater width. This is illustrated in Fig. 7 where the experimental points of $U_{3\omega}$ and φ are plotted against the logarithm of frequency for a 1.5 mm wide Ni heater on a PEEK substrate. The solid lines in Fig. 7 were obtained from a numerical integration of Eq. (5). The calculated curves qualitatively agree with the experimental voltages and phase shifts. The absolute shift of the φ base

line at low frequencies, the step in the φ base lines at the dynamic glass transition, and the small frequency-dependent deviation in our $\Delta(\rho\kappa c_p)'$ data can be explained by Eq. (5): ΔT decreases and φ increases significantly if the thermal wavelength becomes of the order of heater width (especially at low frequencies). For instance, at a heater width of $2b \equiv \lambda = 1.2$ mm, ΔT and, therefore, $U_{3\omega}$ decrease to ca. 60% of the maximum value, and φ increases from $-45°$ to ca. $-23°$ for the case of a Ni heater on a PEEK substrate (see also Fig. 7).

Another relevant problem is the finite *sample* thickness, especially for polymeric glasses, where the samples should be relatively thin because of adhesion problems. We observed some unexpected deviations in the absolute values of $(\rho\kappa c_p)^*$ for very thin samples.

An explanation is obtained from an approach that describes the propagation of temperature waves in a sample of finite thickness (see also [17,18]). The model situation is schematically shown in Fig. 8a. We have a thin nickel layer (being simultaneously heater and thermometer) surrounded by the sample and the substrate. Both layers have a finite thickness,

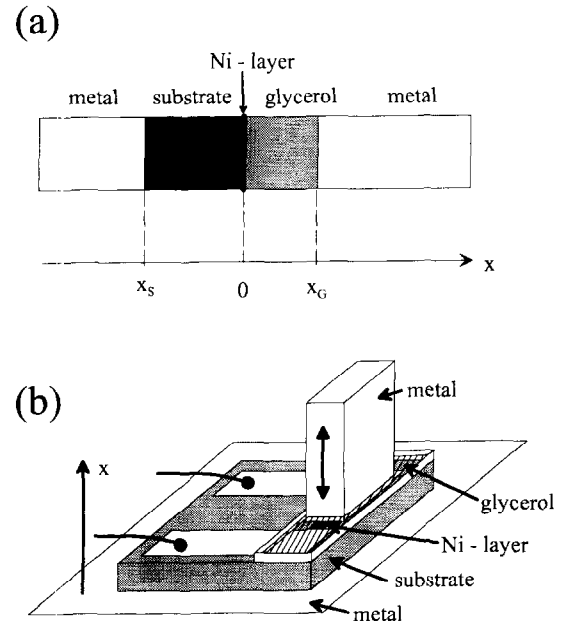

Fig. 8. (a) Schematic diagram of the model geometry for the calculations. The heater is assumed to have infinitesimal thickness. (b) Schematic representation of the experimental cell.

$|x_G|$ for the sample and $|x_S|$ for the substrate. Outside, we have a copper block (modeled here with $\kappa = \infty$, because $\kappa_{Cu} \gg \kappa$ and κ_S) with a given temperature T_R as a reservoir. The general solution of the heat diffusion equation (with separated time dependence) is

$$T(x,t) = A + Bx + \sum_{\omega} e^{-i\omega t}(Ce^{kx} + De^{-kx}) \tag{6}$$

Depending on the material, we have κ, c_p, ρ without index for the sample, $x_G \leq x < 0$, and $\kappa = \kappa_S$, $c_p = c_{p,S}$, $\rho = \rho S$ for the substrate, $0 < x \leq x_S$.

The boundary conditions at the sample-reservoir or substrate-reservoir surface are

$$T(x,t)|_{(x=x_G)} = T(x,t)|_{(x=x_S)} \equiv T_R \tag{7}$$

For the temperature amplitude inside the sample ($x_G \leq x < 0$), it follows from Eq. (6) and Eq. (7)

$$T(x,t) = T_R + T_\Delta\left(1 - \frac{x}{x_G}\right) + \sum_{\omega}\left[\Delta T(\omega)e^{-i\omega t}\frac{\sinh(k(x - x_G))}{\sinh(-kx_G)}\right] \tag{8}$$

where T_Δ is the stationary temperature difference between the Ni layer and the reservoir. The situation inside the substrate ($0 < x \leq x_S$) is obtained by the substitutions $x_G \rightarrow x_S$ and $k \rightarrow k_S$.

The time-dependent temperature at the Ni layer ($x = 0$) is obtained as

$$T_0(t) = T_R + T_\Delta + \sum_{\omega}[\Delta T(\omega)e^{-i\omega t}] \tag{9}$$

and the heat current inside the heater is

$$\frac{P(t)}{A} = \left[\kappa\frac{dT}{dx}\right]_{x\rightarrow -0} - \left[\kappa_S\frac{dT}{dx}\right]_{x\rightarrow +0}$$

$$= T_\Delta\left(\frac{\kappa_S}{x_S} - \frac{\kappa}{x_G}\right) + \sum_{\omega}\left[\Delta T(\omega)e^{-i\omega t}\left(\frac{k\kappa}{\tanh(-kx_G)} - \frac{k_S\kappa_S}{\tanh(-k_Sx_S)}\right)\right] \tag{10}$$

Operating with an input current of frequency $\omega/2$, we

generate the power

$$P(t) = \frac{I_0^2 R_0}{2}(1 + \cos(\omega t)). \tag{11}$$

For the temperature amplitude at the nickel heater ($x = 0$), we obtain

$$\Delta T = \frac{I_0^2 R_0}{2A}\left(\frac{k\kappa}{\tanh(-kx_G)} - \frac{k_S\kappa_S}{\tanh(-k_S x_S)}\right)^{-1} \tag{12}$$

Assuming that the *substrate* thickness is large compared to the thermal wavelength $x_S \gg \lambda_S$, and that the sample is outside the dynamic glass transition ($\delta \equiv 0$ in Eq. (3)) it follows that

$$U_{3\omega}e^{i\varphi} = \frac{\alpha I_0^3 R_0^2}{2A}e^{i\frac{\pi}{4}}\left(\kappa_S|k_S| + \kappa|k|\sqrt{\frac{\cosh(\sqrt{2}|k||x_G|) + \cos(\sqrt{2}|k||x_G|)}{\cosh(\sqrt{2}|k||x_G|) - \cos(\sqrt{2}|k||x_G|)}}e^{i\varepsilon}\right)^{-1} \tag{13}$$

with an additional phase angle

$$\varepsilon = \arctan\left(\frac{\sin(\sqrt{2}|k||x_G|)}{\sinh\sqrt{2}|k||x_G|)}\right) \tag{14}$$

Both the amplitude correction in Eq. (13) and the phase ε depend explicitly on the sample thickness x_G. The situation is much more complicated at the dynamic glass transition. The amplitude correction and ε then depend additionally on the relaxation phase shift δ (see Eq. (3)).

Eq. (13) was checked by a variation of the sample thickness for glycerol at 40°C, i.e. well outside the dynamic glass transition. The experimental cell is schematically presented in Fig. 8b. The nickel heater had an area of ca. $3 \times 4\,mm^2$ and a thickness of ca. 70 nm. The PEEK substrate had a thickness of ca. 5 mm. The sample thickness was varied in the 0.1–2 mm range. The normalized $U_{3\omega}$ signal amplitude is plotted versus sample thickness $|x_G|$ for two frequencies (0.2 and 2 Hz) in Fig. 9. The signal voltage shows an asymptotic value for $|x_G| \gg \sqrt{\kappa/(\omega\rho c_p)}$, an overshot for $|x_G|$ values near the thermal wavelength, and a rapidly decreasing signal for very small thicknesses. Eq. (13) and literature data for κ and ρc_p [19] were used to calculate the dotted $U_{3\omega}(x)$ lines in Fig. 9. The calculated curves qualitatively show the expected shape. The solid lines in Fig. 9 were obtained from a fit of the experimental data using Eq. (13). The fits agree with the experimental data within the experimental uncertainty, but the quantitative agreement between the observed κ and ρc_p values and literature data is poor.

In Table 1 our κ and ρc_p fit data for glycerol are compared to data both from a comparison of wire and plane heater experiments by Birge [11] as well as stationary data for κ and ρc_p. The main reason for this disagreement may arise because our assumptions do not exactly correspond to the experimental setup: The heater was relatively small, the copper blocks on both sides are not infinite, and small tilts cannot be completely excluded. For long heaters, its width should be much larger than the thermal wavelength λ (Fig. 7) in order to ignore heater-size effects. For $\nu = 0.2$ Hz of a heater on PEEK substrate, the wavelength is $\lambda \approx 0.3$ mm, so that a heater size of $3 \times 4\,mm^2$ seems too small to obtain exact values of κ and ρc_p from

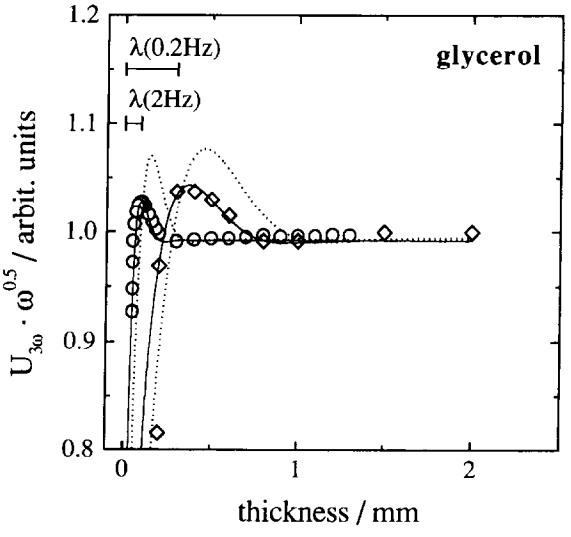

Fig. 9. HCS $U_{3\omega}\sqrt{\omega}$ signal vs. sample thickness $|x_G|$ for glycerol at 40°C. The frequencies are (○) – 2 Hz and (◇) – 0.2 Hz. The dotted lines are calculated from Eq. (13) using the literature data from Table 1[19]. The solid lines are fits to the experimental data using Eq. (13). The fit parameters are also given in Table 1. The bars indicate one full thermal wave length λ for both frequencies as calculated from literature data.

Table 1
Comparison of specific heat ρc_p and thermal conductivity κ data for glycerol

	Fitted from data shown in Fig. 9 at 0.2 Hz	Fitted from data shown in Fig. 9 at 2 Hz	From a comparison of a wire and plane heater experiment [11]	Data from DSC and from Ref. [19]
ρc_p/J cm^{-3} K^{-1}	2.22	2.38	2.8	2.58
κ/W m^{-1} K^{-1}	1.58×10^{-5}	0.95×10^{-5}	3.2×10^{-5}	2.9×10^{-5}
$\rho\kappa c_p$/J^2 cm^{-4} s^{-1} K^{-2}	3.51×10^{-3}	2.26×10^{-3}	8.96×10^{-3}	7.48×10^{-3}

Eq. (13). Nevertheless, the qualitative features of the experimental data can be reproduced by Eqs. (13) and (14). The experiments show that the $(\rho\kappa c_p)^*$ results for glycerol are not disturbed if the sample thickness is larger than three times the thermal wavelength ($\lambda_{\text{glycerol}}(0.2\,\text{Hz}) \approx 0.3$ mm at 40°C).

4. HCS for dynamic glass transition in polymers

This section will present representative experimental HCS results which demonstrate our HCS precision at the dynamic glass transition in polymers. Beside the natural rubber sample discussed, the results for a conventional polydisperse polystyrene (PS) sample and for a random poly(*n*-butyl methacrylate-stat-styrene) copolymer with very small HCS signals are shown. Since the main emphasis of this paper is on the technical aspects, the data are presented only with a brief discussion. The physical aspects will further be discussed in separate papers [7,8,20–24].

The HCS $(\rho\kappa c_p)^*$ output as a function of temperature for the polystyrene sample (PS-168N, BASF AG, $T_g = 103$°C) is shown in Fig. 10. The isochrones behave similar to the natural rubber results of Fig. 5. We see the typical compliance behavior, i.e. a glass step from low $(\rho\kappa c_p)'$ values below to higher values above the dynamic glass temperature T_ν as well as the increase of T_ν with increasing frequency. The increase is similar (≈5–8 K/decade) for both samples (PS and NR). This was expected, since the fragilities $F = T_g/(T_g - T_\infty)$ [15] are not too different ($F_{NR} = 6.8$; $F_{PS} = 6.0$). Another common feature is that the *slope* on the low temperature side (glass) of the dynamic glass transition is steeper than on the high temperature side (melt). Subsequently, the step height $\Delta\rho\kappa c_p(\omega)$ as obtained from a tangent construction decreases with increasing frequency and temperature along the dispersion zone. This effect is outside the

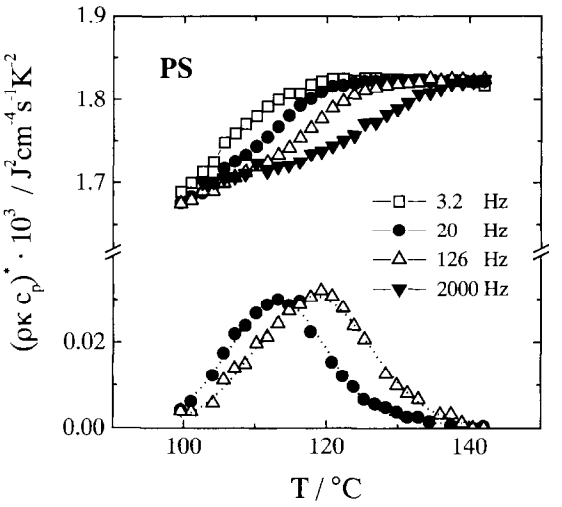

Fig. 10. Real (upper) and imaginary (lower) parts of $(\rho\kappa c_p)^*$ isochrones in polystyrene PS as a function of temperature. The dotted lines in the lower part are fits to the $(\rho\kappa c_p)''$ data with a Gaussian function.

experimental uncertainty (about 10% for $d(\rho\kappa c_p)'/dT$) and was observed for all samples investigated (see also [1]). The spectral width for the temperature sweeps, $\delta T(\omega)$, can be obtained from a fit of the isochronal temperature sweeps with a Gaussian function. Typical values are $\delta T \approx 7$ K for polystyrene and $\delta T \approx 5$ K for natural rubber. The uncertainty of δT is about 10%.

Plots of isothermal $(\rho\kappa c_p)^*$ data for PS vs. logarithm frequency ω are shown in Fig. 11. Symmetrical peaks for $(\rho\kappa c_p)''$ are observed. Corresponding real and imaginary parts of the different isotherms are fitted with common Havriliak–Negami (HN) parameters. The HN shape parameters β and γ are obtained from a superposition of all available isotherms. The values obtained for polystyrene $\beta = 0.65 \pm 0.10$ and $\gamma = 1.14 \pm 0.10$ (very small asymmetry) are similar to the values for natural rubber ($\beta = 0.73 \pm 0.10$,

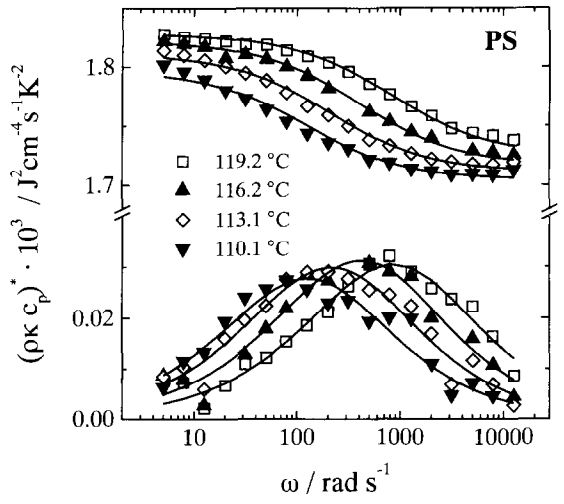

Fig. 11. The real (upper) and imaginary (lower) parts of $(\rho\kappa c_p)^*$ isotherms in polystyrene as function of frequency. The lines in the lower part are fits of the $(\rho\kappa c_p)''$ data with a Havriliak–Negami function. The lines in the upper part were calculated using the same HN parameter set and an additive constant $\rho\kappa c_{poc}$, (Kramers–Kronig consistency test similar to Fig. 6 for NR).

$\gamma = 0.92 \pm 0.10$). The $\Delta(\rho\kappa c_p)$ and ω_{max} values of the different isotherms are of course different.

The experimental situation at the dynamic glass transition is more difficult for PS than for NR: The maximum phase shift $\Delta\varphi$ is significantly smaller, and the relative step height $\Delta(\rho\kappa c_p)/\overline{\rho\kappa c_p}$ is only 25% of the NR value (see Table 2). Nevertheless, the signal-to-noise ratio seems to be large enough to estimate the HN parameters and the spectral width with a high precision.

For the so-called near-onset polymers (see Ref. [20]) poly(*n*-butyl methacrylate) (P*n*BMA) [26,27], poly(*n*-octyl methacrylate) (P*n*OMA) [25,24] and random *n*BMA-stat-styrene copolymers (P(*n*BMA-stat-S)) [21,22] the splitting between the dynamic α glass transition and a local (Goldstein–Johari) β mode, the so-called $\alpha\beta$ splitting, and a nearly linear α onset to zero intensity was dielectrically observed in the kHz range. Simultaneously, the conventional DSC step heights Δc_p at the glass transition became very small. The interpretation suggested is that the cooperative, entropy-active dynamic glass transition α disappears or, inversely, sets on in this region, and Δc_p tends to zero [25]. The small $\Delta c_p/\bar{c}_p$ values are not easy to measure by HCS.

The $(\rho\kappa c_p)^*$ isochrones for a P(*n*BMA-stat-S) copolymer with a styrene content of 19% mol (T_g = 33°C, M_n = 250 kg/mol, M_w/M_n = 2.1) are shown in Fig. 12 as an example for a near-onset polymer. The slope of the glassy and molten state tangents are significantly different again $(d(\rho\kappa c_p)'/dT|_{glass} > d(\rho\kappa c_p)'/dT|_{melt})$, i.e. the step height $\Delta(\rho\kappa c_p)$ decreases with increasing temperature or frequency. The glass transition step in the usual sense seems to disappear in the kHz range, $\Delta(\rho\kappa c_p)$ tends to zero, and what remains seems to be only a bendlike transition. Such a behavior was also observed in DSC experiments for some near-onset polymers such as P*n*OMA or poly(ethylhexyl methacrylate) [25,28]. An onset temperature $T_{on}(\Delta\rho\kappa c_p(T_{on}) = 0)$ can be obtained from an intersection of the linearly extrapolated $(\rho\kappa c_p)'$ tangents of Fig. 12 above and below the dynamic glass transition. The observed T_{on} values are (97 ± 10)°C, nearly independent from the frequency of the isochronal used. The specifics of our data evaluation procedure (see (a) and (b) in Section 2) has no influence on the T_{on} values from the tangent construction. The imaginary part in the lower part of Fig. 12 shows a significant peak at the dynamic glass transition up to 2 kHz. The dispersion $\delta T(2\,\text{kHz}) \approx 15$ K is large as compared to conventional polymers such as NR, PS or polyvinylacetate (PVAC). The peak maximum values decrease with increasing frequencies and temperatures. Unfortunately, the scatter in the $(\rho\kappa c_p)^*$ data is too large to

Table 2
Typical HCS properties of the samples

	Glycerol	NR	PS	P(*n*BMA-stat-S), 19% S
$\overline{\rho\kappa c_p}$(20 Hz)/J^2 cm^{-4} s^{-1} K^{-2}	9.1×10^{-3}[a]	2.2×10^{-3}	1.76×10^{-3}	1.4×10^{-3}
$\Delta(\rho\kappa c_p)/(\overline{\rho\kappa c_p})$ (20 Hz)	0.48	0.25	0.06	0.15 (2kHz)···0.01 (2 Hz) S.Ms.
$\Delta\varphi$(20 Hz)/°	2.6	0.8	0.6	0.4

[a] Absolute error at 20 Hz is about 100%.

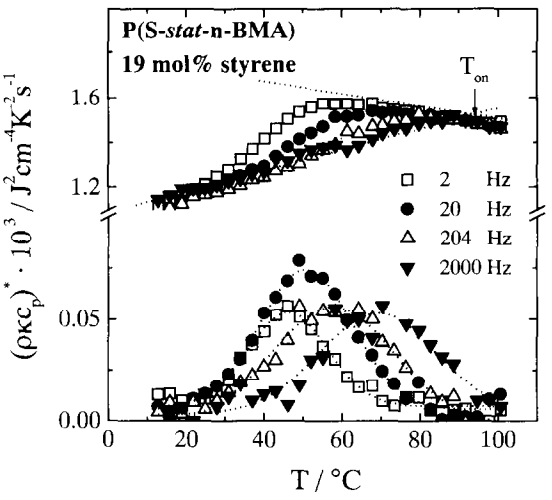

Fig. 12. The real (upper) and imaginary (lower) parts of HCS $(\rho\kappa c_p)^*$ isochrones of a P(S-stat-*n*BMA) copolymer with 19% mol styrene as function of temperature. The dotted lines in the lower part are fits to the $(\rho\kappa c_p)''$ data with a Gaussian function.

present a set of isotherms. The data are not in contradiction to the assumption that the observed isochronal properties are a consequence of an approximately linear decrease of isothermal step heights $\Delta c_p(T)$ in the near-onset region with $\Delta c_p(T) \rightarrow 0$ for $T \rightarrow T_{on}$. The details of such a glass transition onset are discussed elsewhere [23,24].

Table 2 compares typical HCS output parameters for the polymers investigated and glycerol. Both relevant properties, the mean value $\overline{\rho\kappa c_p}(T_\alpha)$ and the relative step height $\Delta(\rho\kappa c_p)/\overline{\rho\kappa c_p}$ are much smaller for our polymers than for glycerol. Nevertheless HCS data for polymers are obtained with a reasonable precision.

5. Conclusion

We have tried to demonstrate the actual possibilities and limits of our heat capacity spectroscopy setup for the investigation of the dynamic glass transition in polymers and other materials. It is now possible to get heat capacity spectra for glass formers with small heat capacity steps down to $\Delta c_p/\overline{c_p}$ of few percent, especially for polymers near the glass transition onset. The spectral width for the temperature sweeps, δT, can be estimated with an uncertainty of about 10 percent from curves similar to Fig. 12, also in the onset region. This is important for an estimation of the characteristic length of glass transition near the onset. The uncertainty of $c_p'(T)$ slopes below and above the dispersion zone is small enough for an estimation of a calorimetric onset temperature [31] defined as the limit, where $\Delta c_p \rightarrow 0$ in an extrapolation.

Acknowledgements

The authors thank Dr. S. Höring and S. Zeeb for the synthesis of the statistical nBMA-*stat*-styrene copolymers and the Continental AG Hannover for providing the rubber sample. This work was supported by the Deutsche Forschungsgemeinschaft, the Fonds der Chemischen Industrie and by the Land Sachsen-Anhalt.

References

[1] N.O. Birge and S.R. Nagel, Phys. Rev. Lett., 54 (1985) 2674.
[2] The asterisk is only used to indicate a complex quantity.
[3] M. Reading, Trends Polym. Sci., 1 (1993) 248.
[4] S. Weyer, A. Hensel, J. Korus, C. Schick, and E. Donth, this isssue.
[5] N.O. Birge, Y.H. Jeong, S.R. Nagel and N.Y. Ann, Acad. Sci., 484 (1986) 101.
[6] S.R. Nagel in NATO ASI Lectures; T. Riste, D. Sherrington Eds.; Geilo, Norway, 1993.
[7] M. Beiner, J. Korus, H. Lockwenz, K. Schröter and E. Donth, Macromolecules, 29 (1996) 5183.
[8] E. Donth, M. Beiner, S. Reissig, J. Korus, S. Garwe, S. Vieweg, S. Kahle, E. Hempel and K. Schröter, Macromolecules, 29 (1996) 6589.
[9] N.O. Birge and S.R. Nagel, Rev. Sci. Inst., 58 (1987) 1464.
[10] D.H. Jung, T.W. Kwon, D.J. Bae, I.K. Moon and Y.H. Jeong, Meas. Sci. Technol., 3 (1992) 475.
[11] N.O. Birge, Phys. Rev. B, 34 (1986) 1631.
[12] P.K. Dixon and S.R. Nagel, Phys. Rev. Lett., 61 (1988) 341.
[13] L.A. Rosenthal, Rev. Sci. Inst., 32 (1961) 1033.
[14] J. Korus, Thesis, Universität Halle, 1997.
[15] E. Donth, Relaxation and Thermodynamics in Polymers. Glass Transition, Akademie-Verlag, Berlin, 1992.
[16] D. Bae, K.B. Lee, J. Jeong, S.M. Lee and S.I. Kwun, J. Korean Phys. Soc., 26 (1993) 137.
[17] R. Frank, V. Dach and J. Fricke, Rev. Sci. Inst., 64 (1993) 760.
[18] J. Morikawa, J. Tan and T. Hashimoto, Polymer, 36 (1995) 4439.
[19] Handbook of Chemistry and Physics; D.R. Lide Ed., 76th Edition, CRC press, New York, 1995-96.
[20] E. Donth, J. Korus, E. Hempel, and M. Beiner, this issue.

[21] E. Donth, J. Polym. Sci., Polym. Phys. Ed., 34 (1996) 2881.
[22] S. Kahle, J. Korus, E. Hempel, R. Unger, and E. Donth, to be published.
[23] J. Korus, E. Hempel, and E. Donth, to be published.
[24] M. Beiner, J. Korus, E. Hempel, and E. Donth, to be published.
[25] E. Hempel, M. Beiner, T. Renner and E. Donth, Acta Polymer., 47 (1996) 525.
[26] F. Garwe, A. Schönhals, M. Beiner, K. Schröter and E. Donth, J. Phys.: Cond. Matter, 6 (1994) 6941.
[27] F. Garwe, A. Schönhals, H. Lockwenz, M. Beiner, K. Schröter and E. Donth, Macromolecules, 29 (1996) 247.
[28] E. Hempel, S. Schlenker, DSC measurements for PEHMA, unpublished results.
[29] M.L. Williams, R.F. Landel and J.D. Ferry, J. Am. Chem. Soc., 77 (1955) 3701.
[30] S. Havriliak and S. Negami, J. Polym. Sci., C14 (1966) 99.
[31] S. Kahle, J. Korus, E. Hempel, R. Unger, S. Höring, K. Schröter, and E. Donth, to be published.